

A Nonempirical Study of Oxygen Adsorption on the (011) In_2O_3 Surface

K. S. Kurmangaleev^{a, *}, T. Yu. Mikhailova^b, and L. I. Trakhtenberg^{a, c}

^a *Semenov Federal Research Center for Chemical Physics, Russian Academy of Sciences, Moscow, 119991 Russia*

^b *Kurnakov Institute of General and Inorganic Chemistry, Russian Academy of Sciences, Moscow, 119991 Russia*

^c *Moscow State University, Moscow, 119991 Russia*

**e-mail: f7033@mail.ru*

Received September 4, 2021; revised December 14, 2021; accepted December 16, 2021

Abstract—Using density-functional calculations, we demonstrate that adsorption of an oxygen molecule on the (011) indium oxide surface with a neutral oxygen vacancy is an activationless process. The stretching frequency of an adsorbed oxygen molecule is calculated for different stable geometries on the indium oxide surface. We simulate scanning tunneling microscopy images of the (011) indium oxide surface: for a stoichiometric surface and a surface with an oxygen vacancy.

Keywords: transparent conductive oxides, oxygen defects, oxygen adsorption, oxidation of indium oxide, scanning tunneling microscopy imaging

DOI: 10.1134/S0020168522030086

INTRODUCTION

Surface properties are known to play a very important role in the use of various nanostructured metal oxide materials. Of special interest among such materials is indium oxide, in particular, because it has found practical application in many devices, such as solar cells [1], gas sensors [2, 3], conductive layers of displays [4], and transistors [5, 6].

Diffraction patterns of indium oxide-based nanomaterials show various peaks corresponding to various shapes of nanoparticles: nanorods, nanoprisms, and others. Characteristically, indium oxide has the following low-index crystallographic surfaces: (010), (100), (111), (110), (00 $\bar{1}$), (001), (101), (011), (1 $\bar{1}1$), (1 $\bar{1}\bar{1}$), (11 $\bar{1}$), and (211) [7–9]. Stability of a particular crystallographic plane depends on its surface energy and decreases in the order (111) > (011) > (211) > (001) [10]. Note that the most stable surfaces, (111) and (011), are nonpolar and would be expected to be less reactive when interacting with surrounding gas molecules.

Consider the surface of nanostructured In_2O_3 film. Oxidation of an $\text{In}_2\text{O}_{3-x}$ surface (where x is oxygen nonstoichiometry of the crystal lattice) as a result of interaction with an oxygen-containing atmosphere involves many elementary reactions: dissociation of adsorbed oxygen molecules and oxygen adsorption in the form of O_2^- superoxide or O_2^{2-} peroxide species and also in the form of O^- and O^{2-} . At temperatures below

150°C in air, molecular oxygen prevails on oxide surfaces, whereas at temperatures above 150°C atomic oxygen prevails [11]. Besides, oxygen species can be incorporated into the structure of bulk materials.

It is well known that real crystal surfaces are inhomogeneous, which leads to the formation of a wide range of adsorption centers differing in both adsorption and reaction properties. Such a center can result from any imperfection of a crystal: extended defects (screw dislocations, steps, and others) or point defects (for example, Frenkel or Mott vacancies). Surface oxygen vacancies produce donor states in indium oxide, with energies just near the conduction band minimum [12]. As a result, room temperature is sufficient for transferring electrons from these states to the conduction band of the semiconductor.

Previously, we considered the simplest point defect—a neutral surface oxygen vacancy—and studied thermodynamic characteristics of adsorption of an oxygen molecule on the (011) indium oxide surface [13]. According to calculation results, an adsorbed oxygen atom forms a strong bond with the indium oxide surface, being incorporated into a biographic trap: a surface oxygen vacancy. In this process, adsorbed oxygen acts as an electron density acceptor.

The purpose of this work is to determine quantities necessary for simulating a sensing process [14]. We calculate the activation energy for oxygen adsorption on the (011) indium oxide surface and stretching frequencies of an adsorbed oxygen molecule. In addition, with allowance for the possibility of direct comparison

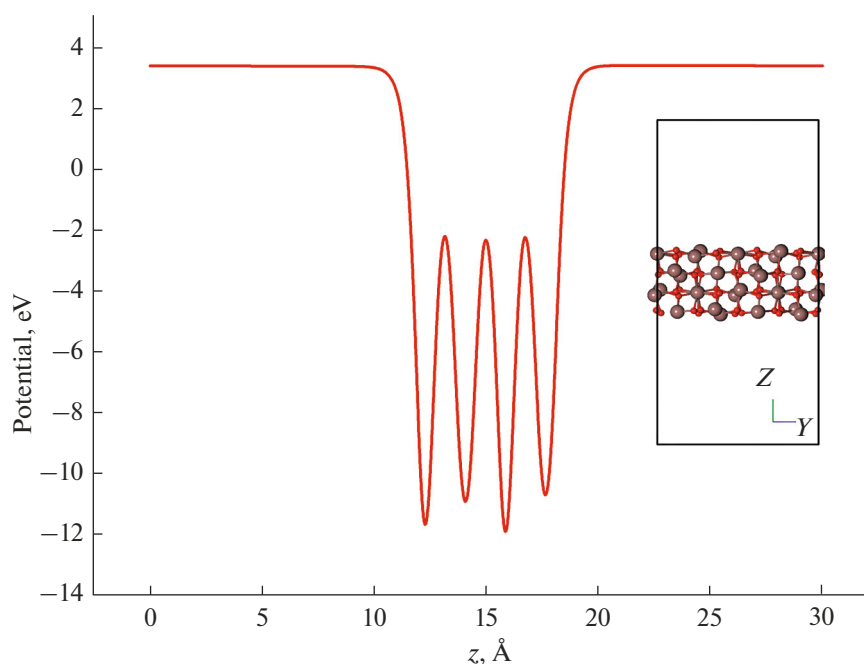


Fig. 1. Shape of the electrostatic potential of an (011) In_2O_3 slab with a neutral surface oxygen vacancy (the potential is averaged in the plane normal to the $0Z$ axis).

with experimental data, we simulate scanning tunneling microscopy (STM) images of both a stoichiometric (011) indium oxide surface and a surface with an oxygen vacancy.

MODEL AND METHODS

An (011) indium oxide surface can terminate with two types of crystallographic planes: (011)- d and (011)- b . These planes are practically similar in the arrangement of oxygen and indium atoms in the structure of their lattice [13], and the (011)- d surface is just $1 \text{ meV}/\text{\AA}^2$ more stable than the (011)- b surface. In our calculations, the (011)- b indium oxide surface is modeled by a slab of four alternating layers, which consist of 32 indium cations and 48 oxygen anions, $10.1171 \times 14.3077 \times 25.9428 \text{ \AA}^3$ in volume. The slab is subject to periodic boundary conditions in all three dimensions, with a vacuum gap on the order of 12 \AA normal to its surface on both sides in order to prevent artificial interaction between periodic images.

Interaction of oxygen and hydrogen molecules with the indium oxide surface was analyzed using density functional theory by the pseudopotential method with a plane-wave basis set at a cutoff energy of 680 eV . Using resources built into the Quantum Espresso (QE) software suite, we performed all necessary spin-polarized calculations in the generalized gradient approximation (GGA) with a PBE exchange correlation functional [15]. In all of our calculations, we used a k -grid constructed by the Monkhorst–Pack method [16] and chose a planar $6 \times 6 \times 1$ grid. All optimization

processes were run until the forces acting on the ions were less than $0.03 \text{ eV}/\text{\AA}$.

Phonon frequencies of adsorbed molecular species at the gamma point were calculated using density functional perturbation theory, whose code is implemented in QE [17]. To visualize all crystal structures, we used Vesta software [18]. If a system has a nonzero total dipole moment, periodic boundary conditions imposed on the system result in artificial interaction between neighboring image dipoles. However, in the case under consideration, the system is nonpolar, as evidenced by the flat electrostatic potential on both sides of the slab (Fig. 1).

At present, there are no scanning tunneling microscopy experimental data for the (011) In_2O_3 crystallographic plane. At the same time, since the (011) In_2O_3 surface is nonpolar, there is low probability that atoms in the immediate vicinity of the surface undergo significant surface changes. In such an approximation, we obtained STM images of stoichiometric and defective (011) In_2O_3 surfaces.

RESULTS AND DISCUSSION

STM images of the In_2O_3 surface. The stoichiometry of oxides can vary as a result of oxidation or reduction processes, which in turn influences not only the structure of the surface but also its electronic properties and interaction with the ambient medium. In the simplest case, certain external conditions (temperature, pressure, and reducing or oxidizing atmosphere)

can lead to the formation of a (1×1) surface structure, which results from a simple section of a unit cell. In particular, heating of metal oxides in a reducing atmosphere rather frequently leads to the formation of single vacancies [19] or associates of a few oxygen vacancies [20] or surface reconstruction. As mentioned above, the (111) and (011) faces of the indium oxide surface are nonpolar. According to Morales et al. [21], the (111) In_2O_3 surface is stoichiometric and has a (1×1) configuration, in agreement with calculations of STM images of empty states in the Tersoff–Hamann approximation [22]. There are still no experimental data on the structure of the (011) In_2O_3 surface. However, since this surface is nonpolar, no significant changes in surface structure would be expected.

STM images of the (011) surface of cubic indium oxide were calculated in the Tersoff–Hamann approximation [22]. For this purpose, we used a denser k -grid, $12 \times 12 \times 1$, constructed by the Monkhorst–Pack method. The image height was chosen so as to obtain the sharpest possible contrast. In all of the figures below, the image height is on the order of 1 \AA from the top surface atom.

Figure 2a shows an STM image of a stoichiometric indium oxide surface at a positive bias voltage of 1 V , where the bright spots correspond to four-coordinate indium cations, and the darker spots, to five-coordinate cations. It is worth noting that the bias voltage 1 V corresponds to the charge density in the energy range 1 eV above the Fermi energy. However, because of the known underestimation of the band gap in calculations in the generalized gradient approximation, charge density calculations at this positive bias voltage include states near the conduction band bottom. Nevertheless, at high positive bias voltages, simulated STM images will be in qualitative agreement with experimental data. As was expected, at a negative bias voltage of -2 V (with allowance for the energy states 2 eV below the Fermi energy) the brightest spots are those corresponding to oxygen anions and the spots corresponding to indium cations, with a major contribution from p -states, are less bright (Fig. 2b).

As to the defective surface (Fig. 3), independent of the applied bias voltage the brightest spots are those corresponding to the indium cations located in the immediate vicinity of a surface defect: a neutral O_4 vacancy [13]. However, at a positive bias voltage there are additional, less bright spots corresponding to indium cations, whereas at a negative bias voltage additional spots correspond to oxygen anions.

Activation energy for oxygen adsorption. The energy of oxygen molecule adsorption on an defective In_2O_3 surface with a neutral oxygen vacancy was calculated previously and was found to be -1.657 and -1.054 eV for horizontal and vertical starting configurations of the axis of the oxygen molecule over the surface, respectively [13]. In particular, Fig. 4 shows the corresponding positions of an oxygen molecule in local

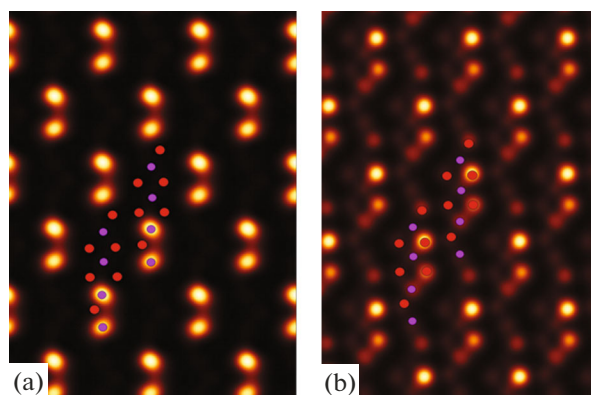


Fig. 2. Simulated STM images of a stoichiometric (011) In_2O_3 surface at bias voltages of (a) $+1$ and (b) -2 V . The colored circles illustrate the arrangement of surface atoms: the lilac circles represent indium cations and the red circles represent oxygen anions.

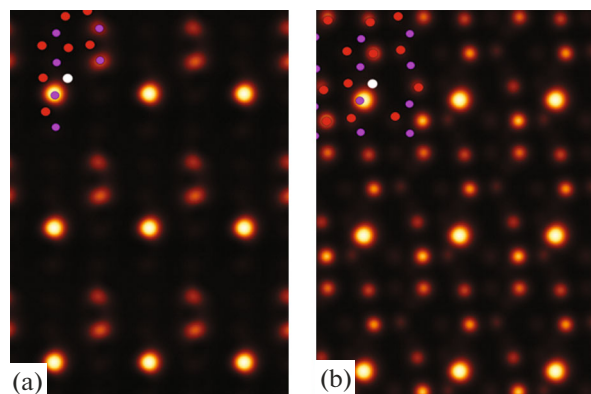


Fig. 3. Simulated STM images of an (011) In_2O_3 surface with a neutral oxygen vacancy at bias voltages of (a) $+1$ and (b) -2 V . The colored circles illustrate the arrangement of surface atoms: the lilac circles represent indium cations, the red circles represent oxygen anions, and the white circle shows the position of an O_4 vacancy [13].

energy minima. In addition, oxygen chemisorbed on a surface was shown to act as an electron acceptor, whereas the indium oxide slab acts as a donor.

To roughly estimate a possible barrier to adsorption, we place an oxygen molecule horizontally along the y axis and vertically at various distances from the surface over a neutral oxygen vacancy. Figure 5 illustrates calculation of the total energy of the slab– O_2 system as a function of the separation between the free oxygen molecule and slab. Even this simple estimate shows that oxygen molecule adsorption is an activationless process. This means that a molecule approaching a surface is merely attracted to it, acting as an acceptor in this process and capturing electrons from the slab. It follows from Fig. 5 that the adsorption energy is -1.26 eV , in approximate agreement with

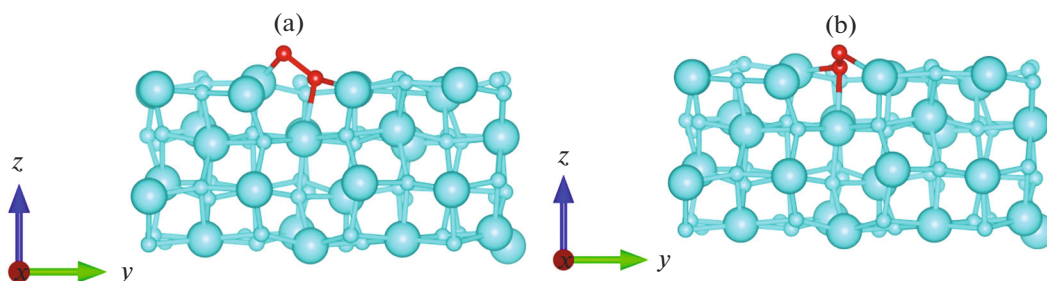


Fig. 4. Equilibrium geometry of an adsorbed oxygen molecule on an defective (011) In_2O_3 surface; the atoms of the oxygen molecule are shown red; the center of mass of both molecules was first placed 2 Å from the topmost atom of the slab; the axis of the molecule is (a) parallel and (b) perpendicular to the slab.

results of more accurate calculations in a previous report [13].

Vibrational frequency of an adsorbed oxygen molecule. To estimate the vibrational frequency of an adsorbed oxygen molecule, we left two top layers of the four-layer slab under consideration (Fig. 4). Calculations were performed only for the gamma point of the Brillouin zone (so called G -approximation) [23, 24]. Such vibrations at $k = 0$ are of particular interest because only them can be observed using infrared and/or Raman spectroscopy in accordance with selection rules. Thus, the approximation in question is one of the most effective ways to selectively study these important regimes.

Phonon creation in a crystal as a result of photon absorption is possible if the laws of conservation of energy and quasi-momentum are fulfilled. Energy characteristics of photons in the infrared spectral region have the same order of frequency as optical

phonons. Optical phonon frequencies in crystals are on the order of 10^{13} s^{-1} , which corresponds to wavelengths from 10 to 100 μm , that is, to the IR spectral region. Since the wavelength of an absorbed photon is many times an interatomic distance, the wave vector of such photons is small compared to the wave vector of phonons in a crystal. It is, therefore, reasonable to expect that photon absorption leads to creation of a phonon with a momentum in the center of the Brillouin zone.

An estimated stretching frequency of a free O_2 molecule is 1558 cm^{-1} , and an experimentally determined value is 1556 cm^{-1} [25]. Oxygen adsorbed on the (011) In_2O_3 surface with a neutral surface oxygen vacancy is an O_2^{2-} peroxide anion. Experimental data for many oxide catalysts demonstrate that the absorption region of IR radiation by bond vibrations in an adsorbed O—O oxygen molecule lies at low frequencies and overlaps with the region of absorption by vibrations in an indium oxide crystal [26]. The calculated phonon frequencies of a slab with an adsorbed O_2 molecule adequately predict changes in stretching frequency; namely, as a result of adsorption, the corresponding frequency of the O_2 molecule becomes redshifted. Indeed, for the stable geometry of an oxygen molecule in Figs. 4a and 4b, we have a frequency of 834.7 and 885.9 cm^{-1} , respectively.

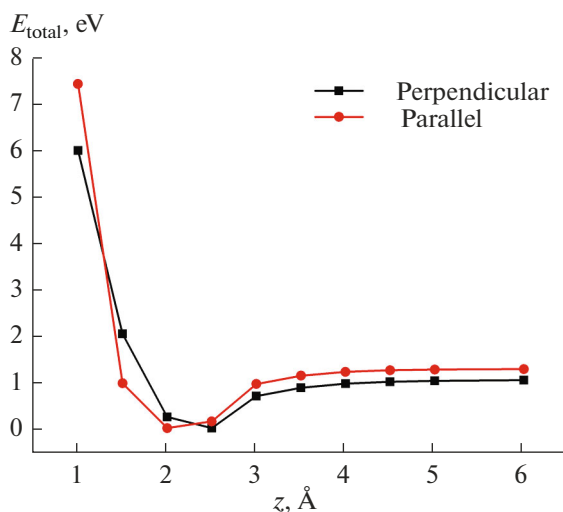


Fig. 5. Total energy of the slab— O_2 system as a function of the separation between the free oxygen molecule and slab (the center of mass of the O_2 molecule was located at various distances from the slab, and the axis of the molecule was perpendicular and parallel to the slab).

CONCLUSIONS

STM images of the (011) In_2O_3 crystallographic plane have been simulated for a stoichiometric surface and a surface with an oxygen vacancy. As expected, in the case of the stoichiometric surface at positive bias voltages, indium cations provide bright contrast because their s — p hybridized states form the conduction band. The energy of these states increases with increasing coordination number, so at a bias voltage of 1 V there is an STM image due to only four-coordinate indium cations, even though all surface cations and anions are located essentially in the same plane.

A different situation holds in the case of negative bias voltages: the bright contrast in the STM image near the valence band maximum (VBM) is due to the p -states of the oxygen anions, with an admixture of the s - and p -states of the indium cations. In addition, the contribution of the s -states of the cations increases with increasing energy separation from the VBM level. An STM image of a surface with a neutral oxygen vacancy at a positive bias voltage typically has a bright spot due to a cation located near the vacancy and two less bright spots due to four-coordinate cations. At negative bias voltages, there are additional contributions from surface oxygen anions.

In addition to simulation of STM images, we have examined oxygen adsorption on a neutral surface oxygen vacancy, followed by the formation of an O_2^{2-} diamagnetic complex. The results suggest that adsorption of an oxygen molecule on the surface of indium oxide with a neutral oxygen vacancy is an activationless process and that the stretching frequency of the adsorbed oxygen molecule is 834.7 and 885.9 cm^{-1} in the two configurations shown in Fig. 4.

In future work, we will examine oxygen adsorption on the (111) In_2O_3 surface with V_{O}^+ vacancies at various coverages and consider interaction of the adsorbed oxygen with atomic and molecular hydrogen. Note that oxygen adsorption on a vacancy is possibly accompanied by the formation of a paramagnetic adsorption complex, whose presence on the surface of indium oxide nanoparticles was demonstrated experimentally [27].

ACKNOWLEDGMENTS

We are grateful to our colleagues at the Joint Supercomputer Center, Russian Academy of Sciences, for providing us with necessary computational resources.

FUNDING

This work was supported by the Russian Federation Ministry of Science and Higher Education (state research target for the Semenov Federal Research Center for Chemical Physics, Russian Academy of Sciences: New Generation of Nanostructured Systems with Unique Functional Properties) and the Russian Foundation for Basic Research (grant nos. 19-37-90016 and 20-07-00158).

CONFLICT OF INTEREST

The authors declare that they have no conflicts of interest.

REFERENCES

1. Untila, G.G., Kost, T.N., and Chebotareva, A.B., ITO/SiO/ n -Si heterojunction solar cell with bifacial 16.6%/14.6% front/rear efficiency produced by ultrasonic spray pyrolysis: effect of conditions of SiO growth by wet-chemical oxidation, *Solar Energy*, 2020, vol. 204, pp. 395–405. <https://doi.org/10.1016/j.solener.2020.04.076>
2. Zhang, D., Liu, Z., Li, C., Tang, T., Liu, X., Han, S., Lei, B., and Zhou, C., Detection of NO_2 down to ppb levels using individual and multiple In_2O_3 nanowire devices, *Nano Lett.*, 2004, vol. 4, no. 10, pp. 1919–1924. <https://doi.org/10.1021/nl0489283>
3. Gerasimov, G.N., Gromov, V.F., Ilegbusi, O.J., and Trakhtenberg, L.I., The mechanisms of sensory phenomena in binary metal-oxide nanocomposites, *Sens. Actuators, B*, 2017, vol. 240, pp. 613–624. <https://doi.org/10.1016/j.snb.2016.09.007>
4. Lee, S., Song, Y., Park, H., Zaslavsky, A., and Paine, D.C., Channel scaling and field-effect mobility extraction in amorphous InZnO thin film transistors, *Solid-State Electron.*, 2017, vol. 135, pp. 94–99. <https://doi.org/10.1016/j.sse.2017.06.033>
5. Dhananjay, Cheng, S.S., Yang, C.Y., Ou, C.W., Chuang, Y.C., Chyi Wu, M., and Chu, C.W., Dependence of channel thickness on the performance of In_2O_3 thin film transistors, *J. Phys. D: Appl. Phys.*, 2008, vol. 41, no. 9, paper 92006. <https://doi.org/10.1088/0022-3727/41/9/092006>
6. Dellis, S., Isakov, I., Kalfagiannis, N., Tetzner, K., Anthopoulos, T., and Koutsogeorgis, D., Rapid laser-induced photochemical conversion of sol–gel precursors to In_2O_3 layers and their application in thin-film transistors, *J. Mater. Chem. C*, 2017, vol. 5, no. 15, p. 3673. <https://doi.org/10.1039/c7tc00169j>
7. Hao, Y., Meng, G., Ye, C., and Zhang, L., Controlled synthesis of In_2O_3 octahedrons and nanowires, *Cryst. Growth Des.*, 2005, vol. 5, no. 4, pp. 1617–1621. <https://doi.org/10.1021/cg050103z>
8. Shi, M., Xu, F., Yu, K., Zhu, Z., and Fang, J., Controllable synthesis of In_2O_3 nanocubes, truncated nanocubes, and symmetric multipods, *J. Phys. Chem. C*, 2007, vol. 111, no. 44, pp. 16267–16271. <https://doi.org/10.1021/jp074445m>
9. Gurlo, A., Nanosensors: towards morphological control of gas sensing activity. SnO_2 , In_2O_3 , ZnO and WO_3 case studies, *Nanoscale*, 2011, vol. 3, no. 1, pp. 154–165. <https://doi.org/10.1039/c0nr00560f>
10. Agoston, P. and Albe, K., Thermodynamic stability, stoichiometry, and electronic structure of bcc- In_2O_3 surfaces, *Phys. Rev. B: Condens. Matter Mater. Phys.*, 2011, vol. 84, paper 045311. <https://doi.org/10.1103/PhysRevB.84.045311>
11. Barsan, N. and Weimar, U., Conduction model of metal oxide gas sensors, *J. Electroceram.*, 2001, vol. 7, pp. 143–167. <https://doi.org/10.1023/a:1014405811371>
12. Lany, S., Zakutayev, A., Mason, T.O., Wager, J.F., Poeppelmeier, K.R., Perkins, J.D., Berry, J.J., Ginley, D.S., and Zunger, A., Surface origin of high conductivities in undoped In_2O_3 thin films, *Phys. Rev. Lett.*, 2012, vol. 108, no. 1, paper 016802. <https://doi.org/10.1103/PhysRevLett.108.016802>
13. Kurmangaleev, K.S., Mikhailova, T.Yu., and Trakhtenberg, L.I., Oxygen chemisorption on the surface of an In_2O_3 (011) nanocrystal, *Inorg. Mater.*, 2020, vol. 56,

- no. 11, pp. 1138–1146.
<https://doi.org/10.1134/S0020168520110060>
14. Bodneva, V.L., Ilegbusi, O.J., Kozhushner, M.A., Kurmangaleev, K.S., Posvyanskii, V.S., and Trakhtenberg, L.I., Modeling of sensor properties for reducing gases and charge distribution in nanostructured oxides: a comparison of theory with experimental data, *Sens. Actuators, B*, 2019, vol. 287, pp. 218–224.
<https://doi.org/10.1016/j.snb.2019.02.034>
 15. Perdew, P., Burke, K., and Ernzerhof, M., Generalized gradient approximation made simple, *Phys. Rev. Lett.*, 1996, vol. 77, pp. 3865–3868.
<https://doi.org/10.1103/PhysRevLett.77.3865>
 16. Monkhorst, H.J. and Pack, J.D., Special points for Brillouin zone integrations, *Phys. Rev. B: Solid State*, 1976, vol. 13, pp. 5188–5192.
<https://doi.org/10.1103/PhysRevB.13.5188>
 17. Baroni, S., de Gironcoli, S., Dal Corso, A., and Giannozzi, P., Phonons and related crystal properties from density functional perturbation theory, *Rev. Mod. Phys.*, 2001, vol. 73, pp. 515–562.
<https://doi.org/10.1103/RevModPhys.73.515>
 18. Momma, K. and Izumi, F., VESTA 3 for three-dimensional visualization of crystal, volumetric and morphology data, *J. Appl. Crystallogr.*, 2011, vol. 44, pp. 1272–1276.
<https://doi.org/10.1107/S0021889811038970>
 19. Lun Pang, C., Lindsay, R., and Thornton, G., Chemical reactions on rutile $\text{TiO}_2(110)$, *Chem. Soc. Rev.*, 2008, vol. 37, no. 10, pp. 2328–2353.
<https://doi.org/10.1039/b719085a>
 20. Dulub, O., Valentin, C.D., Selloni, A., and Diebold, U., Structure, defects, and impurities at the rutile $\text{TiO}_2(011)-(2 \times 1)$ surface: a scanning tunneling microscopy study, *Surf. Sci.*, 2006, vol. 600, no. 19, pp. 4407–4417.
<https://doi.org/10.1016/j.susc.2006.06.042>
 21. Morales, E.H., He, Y., Vinnichenko, M., Delley, B., and Diebold, U., Surface structure of Sn-doped $\text{In}_2\text{O}_3(111)$ thin films by STM, *New J. Phys.*, 2008, vol. 10, paper 125030.
<https://doi.org/10.1088/1367-2630/10/12/125030>
 22. Tersoff, J. and Hamann, D.R., Theory of the scanning tunneling microscope, *Phys. Rev. B: Condens. Matter Mater. Phys.*, 1985, vol. 31, no. 2, pp. 805–813.
<https://doi.org/10.1103/physrevb.31.805>
 23. Ulusoy, I.S., Scribano, Y., Benoit, D.M., Tschetschekin, A., Maurer, N., Koslowski, B., and Ziemann, P., Vibrations of a single adsorbed organic molecule: anharmonicity matters, *Phys. Chem. Chem. Phys.*, 2011, vol. 13, pp. 612–618.
<https://doi.org/10.1039/c0cp01289k>
 24. Keceli, M., Hirata, S., and Yagi, K., First-principles calculations on anharmonic vibrational frequencies of polyethylene and polyacetylene in the gamma approximation, *J. Chem. Phys.*, 2010, vol. 133, no. 3, paper 034110.
<https://doi.org/10.1063/1.3462238>
 25. Nakamoto, K., *Infrared and Raman Spectra of Inorganic and Coordination Compounds*, New York: Wiley, 1978.
<https://doi.org/10.1002/0470027320.s4104>
 26. Davydov, A.A., *Molecular Spectroscopy of Oxide Catalyst Surfaces*, Chichester: Wiley, 2003.
[https://doi.org/10.1016/s1351-4180\(03\)01049-3](https://doi.org/10.1016/s1351-4180(03)01049-3)
 27. Siedl, N., Gügel, P., and Diwald, O., First combined electron paramagnetic resonance and FT-IR spectroscopic evidence for reversible O_2 adsorption on $\text{In}_2\text{O}_{3-x}$ nanoparticles, *J. Phys. Chem. C*, 2013, vol. 117, no. 40, pp. 20722–20729.
<https://doi.org/10.1021/jp4069834>